

# Dynamic Characterization of a Prototype of the Thirty Meter Telescope Primary Segment Assembly

Martin W. Regehr\*<sup>a</sup>, Peter M. Thompson<sup>b</sup>, M. Mark Colavita<sup>a</sup>, James D. Moore<sup>a</sup>  
Mark Sirota<sup>c</sup>, Eric C. Williams<sup>c</sup>

<sup>a</sup>Jet Propulsion Laboratory, California Institute of Technology, 4800 Oak Grove Dr., Pasadena, CA

<sup>b</sup>Systems Technology, Inc., 13766 S. Hawthorne Blvd., Hawthorne, CA 90250

<sup>c</sup>TMT Observatory Corporation, 2632 East Washington Blvd, Pasadena, CA, USA 91107

## ABSTRACT

Finite element models (FEMs) are being used extensively in the design of the Thirty Meter Telescope (TMT). One such use is in the design and analysis of the Primary Segment Assembly (PSA). Each PSA supports one primary mirror segment on the mirror cell, as well as three actuators, which are used to control three degrees of freedom – tip, tilt, and piston – of the mirror segment. The dynamic response of the PSA is important for two reasons: it affects the response of the mirror to fluctuating wind forces, and high-Q modes limit the bandwidth of the control loops which drive the actuators, and impact vibration transmissivity, thereby degrading image quality. We have completed a series of tests on a prototype PSA, in which the dynamic response was tested. We report on the test methods used to measure the dynamic response of the PSA alone and with candidate actuators installed, and we present comparisons between the measured response and FEM predictions. There is good agreement between FEM predictions and measured response over the frequency range within which the dynamic response is critical to control system design.

**Keywords:** Segmented telescope, finite element models, control-structure interaction

## 1. INTRODUCTION

The Thirty Meter Telescope is a segmented primary mirror telescope currently being designed for construction at Mauna Kea in Hawaii.<sup>1</sup> The primary mirror will consist of 492 hexagonal segments.

Each mirror segment is supported on a Segment Support Assembly (SSA); this combination forms a Primary Segment Assembly (PSA), illustrated in Figure 1. The SSA was developed by HYTEC Inc. and was presented in previous papers<sup>2,3</sup>. The three actuators are located at three points under the segment as shown in the figure. Each actuator exerts a force perpendicular to the surface of the segment, the combination making it possible to control three rigid body degrees of freedom of the segment: tip, tilt, and piston. The remaining three degrees of freedom, clocking and translation in the plane of the segment, are passively controlled by the SSA.

The output shaft of the actuator is connected to the moving frame of the SSA, an aluminum weldment to which are connected the whiffletree components that support the mirror segment. The body of the actuator is attached to the fixed frame of the SSA – another aluminum weldment – near the point where the fixed frame of the SSA attaches to the upper layer of the mirror cell that supports all 492 PSAs.

Three nested levels of control maintain the shape and position of the segments forming the primary mirror. The slowest layer of control periodically adjusts the warping harnesses on each mirror segment modifying the force distribution within the whiffletree supports, using information from the Alignment and Phasing System (APS) while observing a bright star, to correct the local figure of the individual segments. This correction of segment figure takes place perhaps once every two weeks, and represents a sampled-data system with such low bandwidth that neither stability nor interaction with structural resonances or with the other layers of control described here is of concern.

The next layer of primary mirror control, known as the global loop controller, controls three of the six rigid body degrees of freedom of each segment: tip, tilt, and piston, using edge sensors on the segments as inputs. Each edge sensor consists of two halves, installed on the opposite sides of the 2.5 mm gap between adjacent pairs of segments. Two such

sensors, i.e., four sensor halves, are installed near the two ends of each such gap. The global loop controller sends commands to three actuators on each segment to maintain, as nearly as possible, all of the segments flush with their neighbors at the edges they share to within a few nm RMS. This loop operates at approximately 1 Hz.

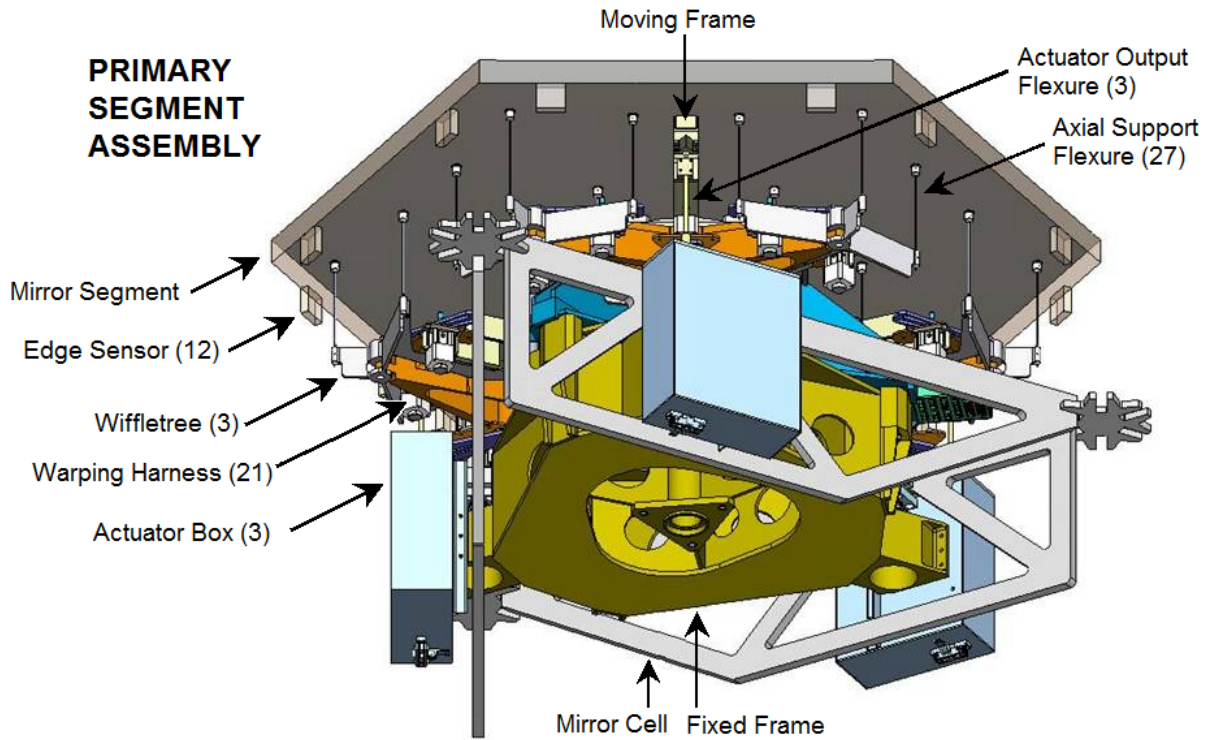


Figure 1 Primary Segment Assembly

The third and fastest layer of control is implemented locally inside each actuator. In general, the actuator contains a force or displacement source and an encoder the actuator measures the local position of the actuator; a control loop is used to feed back from this sensor to the force or displacement source so that the actuator follows position commands sent by the global loop controller. This loop operates at approximately 10 Hz.

When the work described here was performed, three candidate actuator designs were under consideration: a PZT/motor conventional technology (CT) actuator with motorized off-loader, developed by JPL, a “piezo-pump” (PP) hydraulic-type actuator, developed by The Pilot Group, and a voice coil (VC) with motorized off-loader actuator, developed by Marjan Research.

The principal advantage of the soft VC actuator is that it is compliant at high frequencies and therefore has a much lower transmission of mirror cell vibrations to the mirror segments. The hard CT and PP actuators have the advantage that they are stiffer at low frequency and so are more effective at resisting the distorting effects of wind forces on the mirror segments.<sup>4,5</sup>

The VC actuator includes a voice coil, preload springs, and a slow offload mechanism, connected to an output shaft via a set of linkages and flexures. Local feedback in the VC actuator can be used to stiffen it actively at low frequency but the achievable gain is limited by high-Q resonant peaks in the mechanical response of the PSA, and of the mirror cell, which provides the reaction mass against which the actuators push. Both of these mechanical response functions have been calculated using FEMs. Indeed, measurements of the mechanical response of the mirror cell won’t be possible until construction has begun. Additional stability considerations derive from Control Structure Interaction among the various actuators as coupled via the mirror cell.<sup>6-7</sup>

## 2. MEASUREMENT PROCEDURES

The principal purpose of characterizing the PSA was to verify that the FEM was generating results of adequate fidelity for this assembly. FEMs have been and continue to be used extensively for control system design and to predict the performance of the primary mirror.

Figure 2a shows the prototype PSA, which uses an aluminum mass-simulator in place of the glass mirror segment. The holes in the hexagonal sides were drilled so that the mass of the aluminum blank matches the weight of a glass segment. The PSA is installed in a triangular truss structure shown separately in Figure 2c and known as the mirror cell triangle. The mirror cell triangle is similar to the corresponding structure shown in Figure 1, but modified slightly to make it suitable for use on an optical table, the arrangement in Figure 2a. Three simple “dummy” actuators, containing voice coils and off-load springs, were used for the testing. A close-up photo of one of these is shown in Figure 2b; two of the actuators are visible in Figure 2a. These voice coil test actuators were used to characterize the response of the structure as seen by the servo control system. Shaker actuators were also used for dynamic characterization. To measure the effect of disturbance forces entering from the mirror cell, the shaker is set up to push on the mirror cell triangle; the resulting response at the mirror surface represents the transmitted vibration response. To enable the shaker to produce significant mirror cell triangle motion, the triangle is supported at two corners by a short metal post and at one corner by a compliant machinery mount, as shown in Figure 2e.

The dummy actuators were first characterized in the actuator test stand, not shown; a test fixture in which the actuators were loaded with a stack of six 25-lb weights totaling 150 lbs. The motion of actuator was measured, as well as the drive current in the actuator, as a function of frequency. Motion was measured using a Polytech laser interferometer, with a model OFV-353 head and an OFV-3001 controller. The laser interferometer can be seen in Figure 2a and Figure 2d. Motion was also measured using a Honeywell QA 1200 accelerometer, which can be seen at the top of Figure 2d.

An Agilent model 35670A dynamic signal analyzer was used in the step-dwell mode using sine-wave inputs. Actuator drive current was measured on one channel indirectly by measuring the voltage across a 0.51  $\Omega$  current sense resistor connected in series with the actuator voice coil. Measuring drive current, as opposed to voltage, eliminates the effects of the frequency-dependent impedance of the voice coil due to inductance and back-emf. The second channel of the signal analyzer was connected to either the laser interferometer or the accelerometer output voltage. The signal analyzer automatically steps through a set of frequencies, dwelling at each long enough (approximately 20 cycles) for the system to settle and then record a measurement. If the dwell time is not long enough, settling from the previous frequency may contaminate the measurement, a potential problem for lightly damped mechanical systems such as the PSA.

## 3. DYNAMIC MODEL

The measured frequency responses are compared with predicted responses obtained from a dynamic model. Separate models are available for the PSA and the optical table upon which the PSA is mounted. The two separate models can be combined into a single model. The optical table model was found to be necessary for better fitting of the measured data.

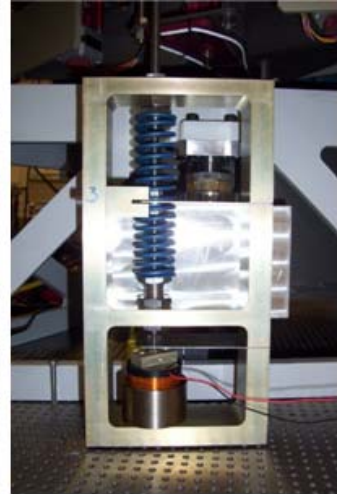
### *PSA FE Model*

A detailed finite element (FE) model of the PSA was developed by HYTEC and used as part of the mechanical design effort. An image showing the mesh is in Figure 3. The FE model represents the mass and stiffness of all major mechanical components in the PSA. The model parameters were estimated using material properties that match the prototype design in Figure 1. The model was developed with high-fidelity so as to be useful for optical performance prediction (gravity and thermal distortion), as well as dynamics and controls simulations. The mirror segment mass properties and mode shapes represent the aluminum blank used in the prototype and not the stiffer glass mirror segment that will be eventually mounted on the production version. The test-specific mirror cell triangle is also included in the FE model. A static test was conducted on the prototype to determine the vertical stiffness at different points on the structure. This data was used to adjust the corresponding model material properties so that the results agreed.

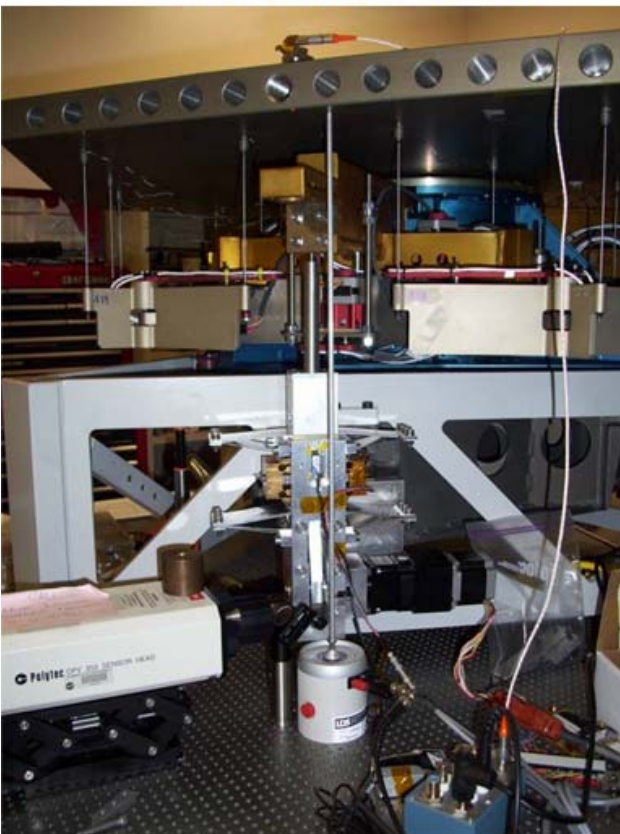
A reduced order model was derived from the full NASTRAN model using Craig-Bampton dynamic reduction. The reduced order model includes 261 modes (up to 350 Hz) and 27 physical nodes. The nodes used for collocated inputs and outputs include the actuator connection to the fixed frame, the actuator output flexure connection to the moving frame, the feet of the mirror cell triangle, and thirteen different locations on the mirror surface. The matrices from the reduced order model were transferred to Matlab, and it is in the Matlab environment that the model frequency responses are computed and compared with the measured responses.



a) Prototype PSA on optical table



b) Dummy actuator with voice coil and offload springs visible



d) Shaker with push rod used for mirror cell response, laser interferometer and accelerometers are visible



c) Mirror cell triangle



e) Alternative supports for mirror cell triangle, stainless steel post & yellow machinery mount

Figure 2 PSA Test Setup

The PSA node locations and several of the mode shapes from the reduced model are shown in Figure 4. In the piston and tip-tilt modes the moving frame and mirror segment move together and the respective frequencies (8.1 and 9.1 Hz) are primarily determined by the total moving mass and the offload spring. In the differential modes the moving frame and mirror segment move in opposite directions and the respective frequencies (156 and 105 Hz) are primary determined by the structural stiffness and the relative mass of the moving frame and mirror segment. The tip-tilt differential (105 Hz) is coupled with a significant amount of mirror bending. This coupling is expected to be much less when the aluminum mirror blank is replaced by the stiffer glass structure. The side-to-side lollipop mode (33 Hz) is unobservable to the servo encoder and so is not controlled. The PSA tower is designed to passively limit the lateral motion.

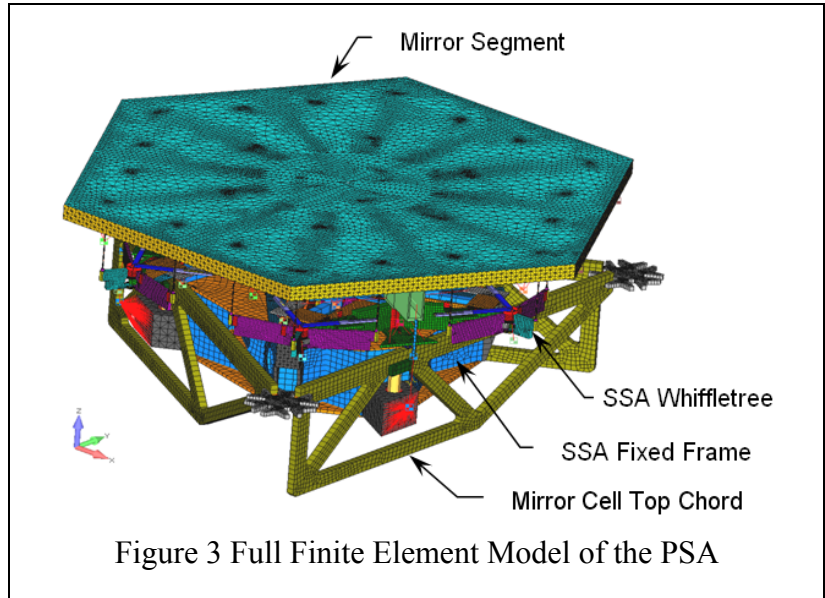


Figure 3 Full Finite Element Model of the PSA

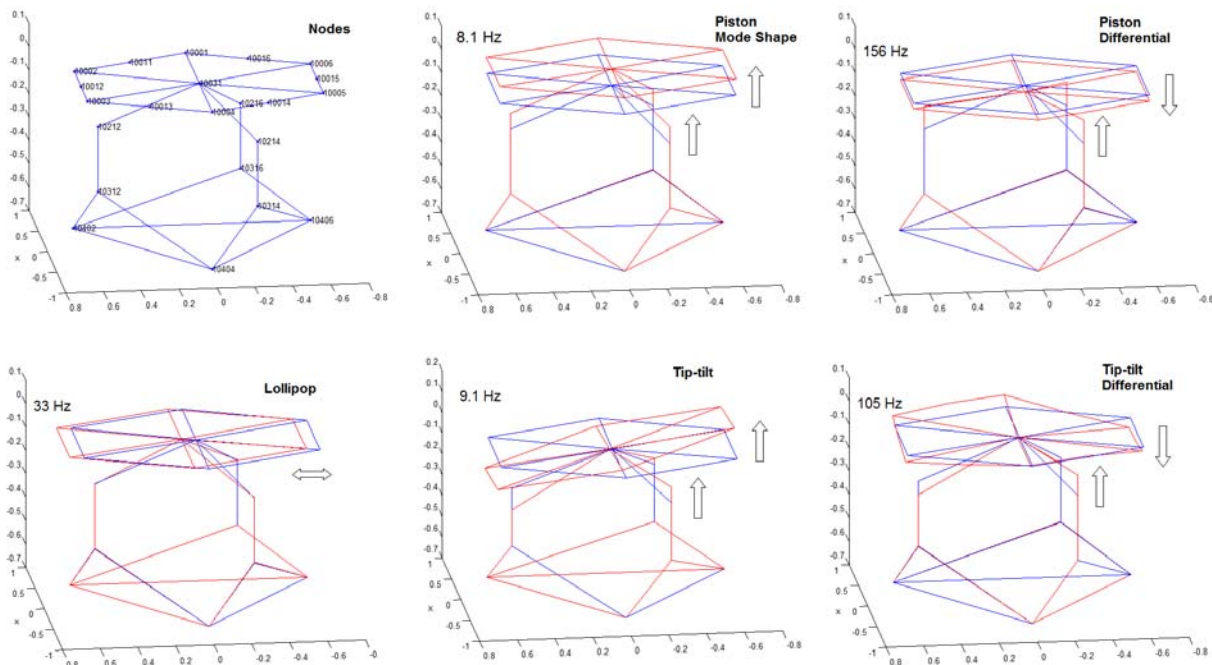


Figure 4 PSA Reduced Dynamic Model Mode Shapes

### Optical Table Model

A rigid body model of the optical table was developed as part of this project. The table model has piston, tip, and tilt modes. The total mass was estimated from the table vendor’s documentation. The pneumatic table legs were modeled as a spring with the spring constant and damping estimated from the vendor data. Automatic table leveling operates at a lower frequency than the test signals ( $\ll 1$  Hz) and is not included in the model. Further information about the table model is in Appendix A.

## Sensors and Actuators

Each of the sensors (accelerometer or laser interferometer) and test actuators (dummy actuator and shaker) is modeled as a scale factor than converts the measured response to volts. The dynamics of the sensor and test actuators are not included in the model, with one exception. Accelerometer measurements have a time delay estimated to be 0.3 milliseconds (10.8 degrees of phase lag at 100 Hz). This time delay is inverted and then acceleration is converted to position by dividing the acceleration frequency response by  $(j2\pi f)^2$ .

## Signals and Systems

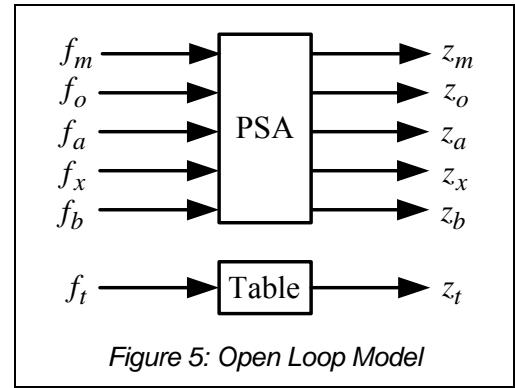
The FE model has the differential form  $M\ddot{x} + Kx = f$ , where  $M$  and  $K$  are respectively the mass and stiffness matrices, the physical state  $x$  contains degrees of freedom at each node, and  $f$  contains the corresponding forces and torques applied at each node. The modal form of the FE model is

$$\ddot{u} + 2\zeta\Omega\dot{u} + \Omega^2u = \Phi^T f, \quad x = \Phi u,$$

where  $\Omega$  is a diagonal matrix with the mode frequencies, the columns of  $\Phi$  are the eigenvectors, also called mode shapes, and  $u$  is the normalized state vector. To make the modal form more compact only a subset of the physical state is included in the output. For the vertical displacement of the nodes shown in Figure 4,  $u$  and  $x$  are  $22 \times 1$  and  $\Phi$  is  $22 \times 261$ . Modal damping is set using the damping ratio  $\zeta$ , which can in general differ for each mode. In this work the PSA modes have  $\zeta = 0.005$  (0.5%) and the table modes have  $\zeta = 0.22$  (22%).

Transfer function blocks of the open loop PSA and table models are shown in Figure 5. The signals are:

- $f_m, z_m$  = mirror vertical force and translation  
(nodes 10012,4,6, each vector is  $3 \times 1$ )
- $f_o, z_o$  = moving frame location outboard of piston attachment  
(each vector is  $3 \times 1$ )
- $f_a, z_a$  = actuator piston attachment on moving frame  
(nodes 10212,4,6, each vector is  $3 \times 1$ )
- $f_x, z_x$  = actuator attachment on fixed frame  
(nodes 10312,4,6, each vector is  $3 \times 1$ )
- $f_b, z_b$  = mirror cell triangle base points  
(nodes 10402,4,6, each vector is  $3 \times 1$ )
- $f_t, z_t$  = table top locations underneath base points  
(each vector is  $3 \times 1$ )



The closed loop version of the PSA and table models is in Figure 6. Relative versions of the signals are needed because each applied force has a reaction force and each measurement is relative to the table. Relative signals are denoted by two letter subscripts, for example  $f_{mt} = f_m - f_t$  is a force applied to the moving frame with a reaction force on the table, and  $z_{mt} = z_m - z_t$  is the corresponding position of the moving frame relative to the table. There is a three-fold symmetry to the PSA, and the bold lines in Figure 6 are vector signals of size  $3 \times 1$ . The applied forces ( $f_1, f_2, f_3$ ) and the measurements ( $z_1, z_2, z_3$ ) are in just one of the three channels.

The closed loop block diagram has four feedback loops:

**Base connection:** a stiff spring that connects the mirror cell triangle to the table, except for the vibration measurements, where this connection is the much less stiff machinery mount.

**Offload:** The springs that hold up the moving frame, plus damping and (if present) the lever reflected mass.

**Servo:** The position controller is connected in the tests to just one of the actuator locations. The other locations are supported by non-powered dummy actuators or stiff rods.

**Mirror correction:** A change in the mirror dynamics included to improve the match between the actuator response model and data.

To model the PSA on a rigid base (no table) constrain  $z_b = z_t = 0$ .



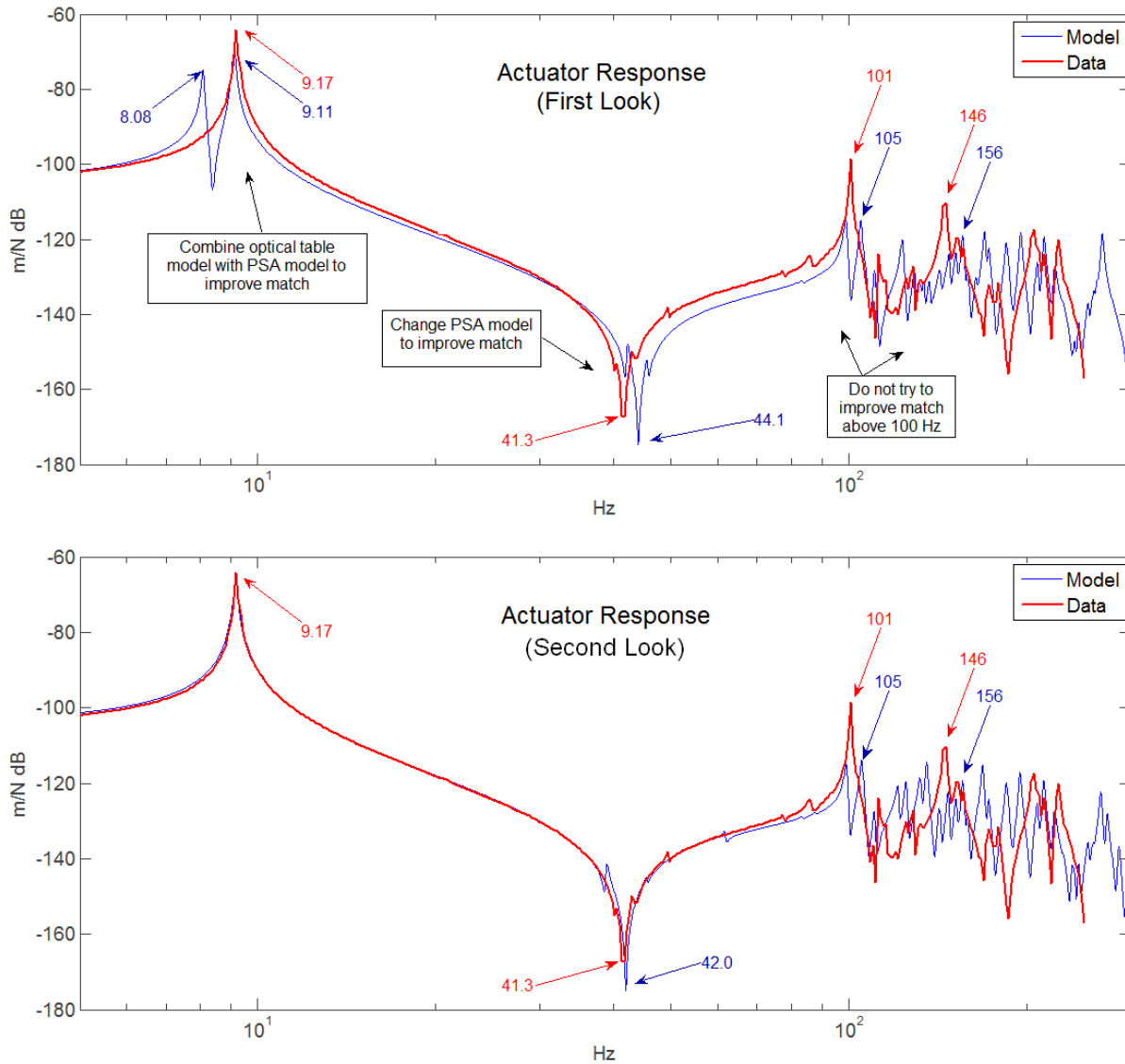


Figure 7: Actuator Response

### Second Look

The second look data includes the optical table model, which is merged with the PSA, and also some system tuning, as described below. The main effect is to move the piston mode of the combined model from 8.08 Hz up to about 9.1 Hz, resulting in a coalescing of the piston and tip-tilt modes and good agreement with the measured data. The optical table that was used is actually three standard optical tables bolted together for a total mass of 2400 kg, more than ten times the mass of the PSA and mirror cell triangle, enough so that changes in the PSA response were expected to be less than about one percent. A surprising outcome of developing the table model was that the “effective mass” of the table is only about 600 kg, i.e., only about three times the mass of the experimental object, and a low enough ratio to cause more than a ten percent change in the PSA piston mode. The same effect can happen in the tip-tilt direction, but the “effective moment of inertia” of the table is much larger than the total moment of inertia of the PSA and as a result there is no significant change in the measured tip-tilt mode of the PSA. The “effective mass” of the table equals the total mass only when the PSA is at the table center-of-mass and then decreases to about one-seventh at the edge. The table is shared with different projects, and the location allocated to the telescope controls team was close to an edge, and by happenstance this location was just the right place to cause the measured piston and tip-tilt modes to line up. Mystery solved.

The model was further improved by including a mirror correction term. The structural spring was increased by 6% and the mass increased by 8%, both just in the tip-tilt directions. These adjustments were made in an ad-hoc manner until the zero locations lined up. There are no static measurements of the PSA in the tip-tilt direction to verify these changes.

### ***What is Close Enough?***

The match between the model and data is “close enough” if the control system is robust to the changes, in other words, if the performance requirements of the position servo are satisfied for a set of models large enough to include the measured response. It is known, for example, that differences in the 10 Hz range are not significant, because the position gain of the servo acts the same as the offload spring and is much larger, and so whether or not the piston and tip-tilt modes coalesce in the open loop model does not matter. Even so, as a matter of principle, the first mode of a system ought to be well understood.

The frequency range where a close match is the most important is 10 to 40 Hz. In this range the loop gain of the combined controller and system is close to unity and therefore the closed loop stability and performance are sensitive to changes in this frequency range. The significantly higher gain of the measured response at 100 Hz is a concern. Appropriate changes can be made to the servo to prevent oscillation of this mode, but some performance may be lost. Whether or not the differences between the data and model above 100 Hz are important depends on the control strategy. In a “gain stable” strategy the loop gain is kept well below unity in this range and so the difference is not important. In a “phase stable” strategy the loop gain can be close to or even above unity in this frequency range, and what becomes more important is whether or not the phase stays between 0 and  $-180$  degrees, in other words, whether or not the response is collocated. The phase plots are not included, but yes, the response is collocated, and so a phase stable strategy is possible.

## **5. MIRROR RESPONSE**

The mirror response is  $z_2 / f_2$  as defined in the Figure 6 block diagram. The model and data responses are compared in each part of Figure 8. The mirror response is the piston motion of the mirror segment due to a disturbance on the mirror that originates at the mirror optical surface. This response is also called the mechanical admittance. The primary source of this disturbance during telescope operation is the wind. Most of the wind energy is at low frequency, and the gain of the mirror response below about 1 Hz determines how stiff the system is with respect to the wind. A wind model used in performance analysis is a von Karman response with a break frequency at about 0.1 Hz. The plots in Figure 8 are the response of the structure and not the power spectra of the mirror response due to a given wind model.

The test setup is shown in Figure 2d. The input force due to the shaker is transmitted through the push rod. The mirror segment vertical response is measured close to the push rod location. Measurements for different tests are made either with the laser or with the accelerometer and then averaged together. The moving frame is supported by dummy actuators at two locations and by a prototype actuator at the third location. The position servo that is part of the prototype actuator is turned on during the tests.

The two parts of Figure 8 use different actuators, the voice coil actuator (VC) and the conventional technology piezo actuator (CT). Moving from low to high frequency across the responses: 1) The low frequency response below about 1 Hz for the VC actuator depends primarily on the integral gain of the position servo, and for the CT actuator it depends primarily on the inherent uncontrolled stiffness of the actuator. There is about a 5% low frequency gain error in the model of the CT actuator. 2) The measured response at about 9 Hz is the “bleed through” of the dummy actuators and would not be present if the test setup were symmetric, in other words if three prototype actuators were used. 3) The peak response at 20.4 and 34.6 Hz is not important for the mirror response because there is little input energy at these frequencies.

## **6. VIBRATION TRANSMISSION**

The vibration transmission is  $z_2 / z_3$  as defined in the Figure 6 block diagram. This response is computed as the ratio of two force-to-position responses:  $(z_2 / f_3) / (z_3 / f_3)$ . The model and measured data are compared in Figure 9. Mirror motion due to vibration is caused by disturbances that originate below the PSA structure. The disturbances give rise to a motion  $z_3$  at the base of the PSA. The vibration transmission plot is a measure of how much the base motion is amplified or attenuated by the PSA structure.

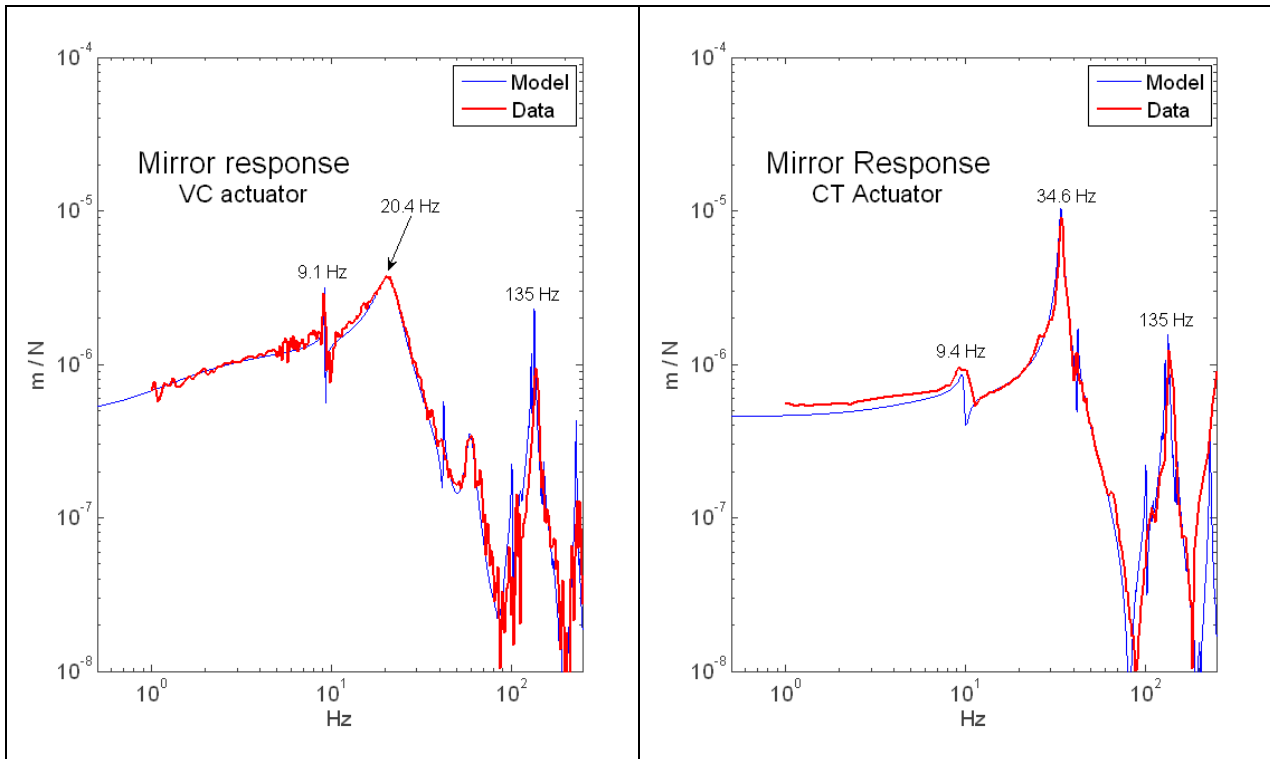


Figure 8: Mirror Response (Wind Disturbance)

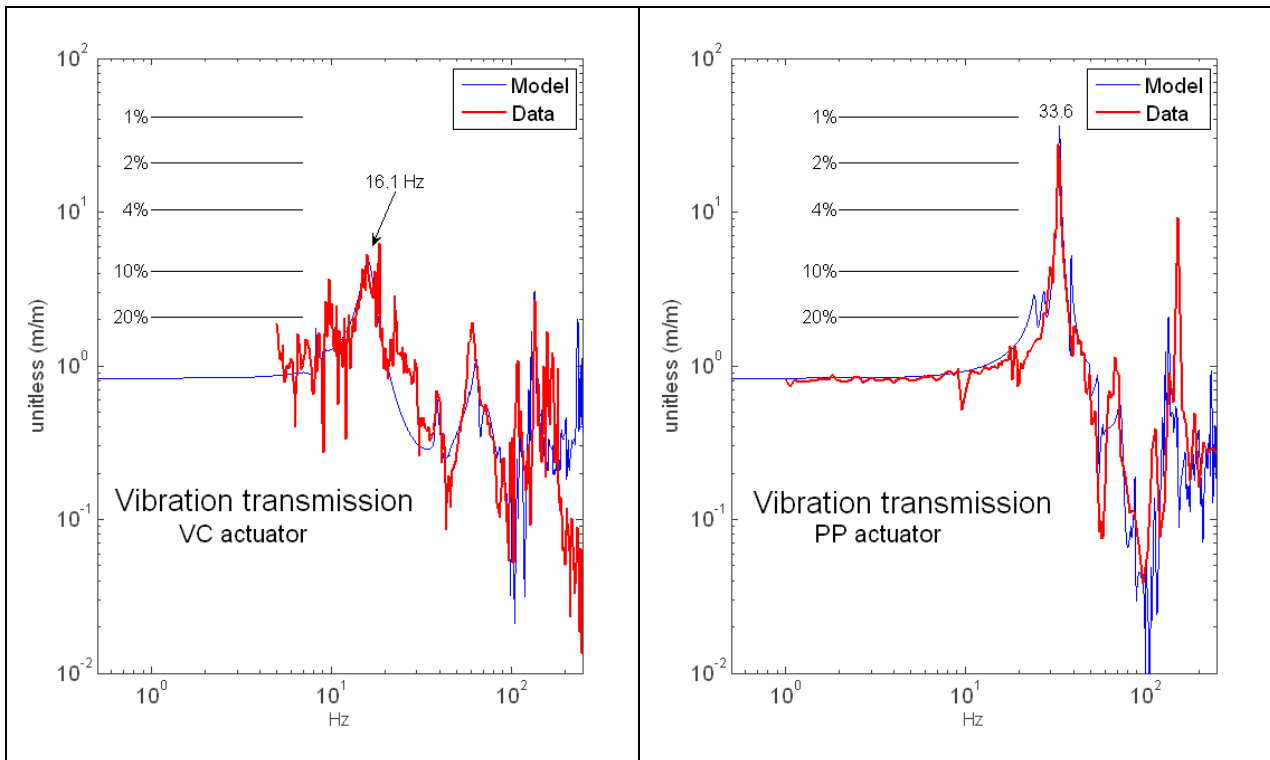


Figure 9: Vibration Transmission

In the experimental setup a force is applied to the mirror cell triangle and then measured at two locations: on the mirror cell triangle and on the mirror. For the vibration test, two corners of the mirror cell triangle sat on short 1.5” diameter stainless steel posts, while the corner nearest the actuator was supported by a Barry model LM1-B machinery mount. This machinery mount incorporates an elastomeric foot that allows the triangle to move in response to a force applied by the shaker. Figure 2e shows one corner of the mirror cell triangle supported by both a post and machinery mount. To shake this corner of the triangle then remove the post, which transfers the weight the post carried to the machinery mount. The shaker is not shown in this figure.

The basic shape of the vibration transmission responses is consistent with what is expected for a structure such as the PSA. At low frequency the gain is close to unity, which means low frequency vibrations pass through the structure, and the base and mirror move together. The response peaks at the fundamental frequency of the structure. The “effective spring constant” and the total moving mass of the PSA primarily determine this frequency. The “effective spring constant” is the servo position gain plus the offload spring constant, which for the VC actuator is primarily determined by the servo gain, and for both the CT and PP actuators is determined primarily by the stiffness of the piezo material. The damping of the fundamental mode is important because it determines the amplification of the vibration in this narrow frequency range. Damping lines are drawn on the plots, equal to equal to  $1/(2\zeta)$  times the low frequency gain, where  $\zeta$  is the damping ratio. For example, 1% damping has  $\zeta = 0.01$  and a vibration amplification of 50. The measured voice coil response, even though it is quite noisy, clearly has significantly better damping than the piezo actuator. On the plot the voice coil damping is just under 10%. Modifications have been made to the voice coil servo to improve this damping to better than 20%. The piezo damping in this measurement is between 1 and 2%. The position servo is not effective in this case at increasing damping because the dominant vibration path is through the offload mechanism. Damping can however be improved by adding an inner loop force feedback. Force feedback was examined as part of the design effort and damping better than 10% was verified experimentally for both (CT and PP) piezo actuators.

## 7. CONCLUSIONS

Frequency response measurement procedures were implemented to provide good signal to noise ratio over the frequency range from 1 to 250 Hz with position motions in the micron range.

Model matches are considered very good (1 to 2% magnitude errors) for the actuator response up to 100 Hz, and good (10% magnitude errors) for the mirror response and vibration responses. The dominant frequencies are matched very well (1 to 2% errors). There are narrow frequency ranges under 100 Hz where larger magnitude errors have occurred. The matches above 100 Hz are not as close but both the magnitude and phase responses have the same general shape.

In order to do this well there has been some tuning of the model parameters, such as the offload stiffness values, to obtain good matches with the magnitudes and the fundamental frequencies. This kind of adjustment is justified because the sensitivity of the frequency response to the parameters is well understood.

There are aspects of the dynamic model recommended for future analysis. 1) The location of the locked actuator zero depends primarily on the mirror segment spring and mass in the tip-tilt direction. Static measurements of these values can be used to provide a better match with the dynamic measurements. To date the static measurements have just been in the piston direction. 2) The influence of the underlying table needs to be better understood. Including the table provided a dramatically better match with the actuator response, but the same improvement was not observed when comparing the mirror response and vibration response. This interaction is a simple version of control structure interaction, which is known to be important for the complete telescope. The optical table is not a good surrogate for the telescope mirror cell structure, because the telescope mirror cell is much stiffer and has several dominant frequencies all higher than the fundamental table frequency of about 1 Hz. Nevertheless a better understanding of the simple test-version of the problem will reduce the risk for the upcoming complicated version, the telescope system. 3) The vibration transmission fit between model and data is good for the dominant frequency and damping ratios although larger errors are observed in narrow frequency bands

Is the model and data comparison good enough? Yes. The controls team has made the conclusion that the model of the PSA provides a good basis for comparing different actuators and for predicting the response of 492 mirror segments when mounted on the TMT mirror cell.

## APPENDIX A: OPTICAL TABLE MODEL

The PSA is attached to a mirror cell triangle which is in turn mounted on an optical table. An optical table is designed to reduce vibration transmission from sources such as foot traffic in the clean room, rotating machinery in adjacent rooms, and truck traffic outside the building. In order to do this the table has a large mass and the table legs are relatively soft springs so that the dominant frequency is in the 1 Hz range. The table has a pneumatic servo that provides automatic leveling, and several mechanisms are implemented to increase the damping of the table modes near 1 Hz and at higher resonant modes. A picture of the optical table from the manufacture's literature is in Figure 10.



In the laboratory that was used for the study there are three tables rigidly attached and arranged as shown in Figure 11a. A dynamic model was developed for this study that includes three rigid body modes: vertical translation and rotation about the horizontal axes. Each table top is considered a rigid rectangle with known mass and moment of inertia matrix. An individual table has a mass of 800 kg and table top dimensions 8 ft by 5 ft by 18 inches. The three table tops are combined using the parallel axis rule. Each table leg is modeled as a spring to ground with  $k = 24000$  N/m and the damping of the table resonant modes is approximated to be 22%. The spring and damping values were obtained by measuring the vertical force to position response at one point on the table. The center-of-mass of the table using the axis system defined in Figure 11a is  $r_{cm} = (1.85, 0.75, -0.229)$  m. The PSA location is shown in Figure 11a. The center point is  $r = (4.05, 0.75, 0)$  m and the radius of the PSA is 0.72 m.

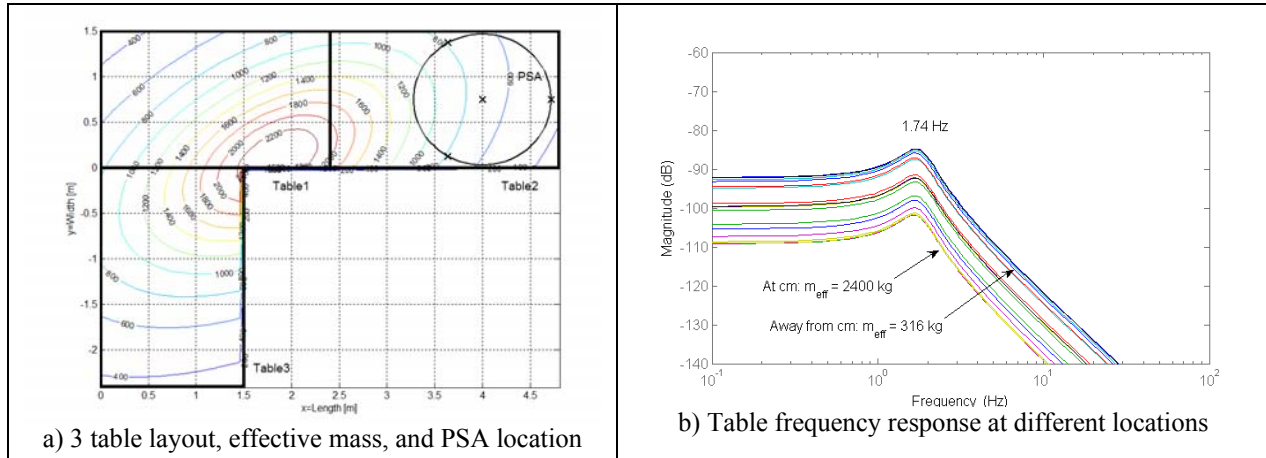


Figure 11: Optical Table Analysis

The dynamic model in finite element form is  $(Ms^2 + K)x = f$ , where

$$M = \begin{bmatrix} 2400 & 0 & 0 \\ 0 & 2754 & -1716 \\ 0 & -1716 & 4716 \end{bmatrix} \text{ kg}, \quad K = \begin{bmatrix} 0.288 & 0 & 0 \\ 0 & 0.345 & -0.206 \\ 0 & -0.206 & 0.583 \end{bmatrix} \text{ N/micron}, \quad x = \begin{bmatrix} z_{cm} \\ \phi_x \\ \phi_y \end{bmatrix} \begin{matrix} \text{m} \\ \text{rad/sec} \\ \text{rad/sec} \end{matrix}$$

The vertical translation is at the center of mass. The vertical force-to-position response for a point  $r_i = (x_i, y_i, 0)$  on the table top relative to the center-of-mass is  $z_i / f_i = c (Ms^2 + Bs + K)^{-1} c^T$ , where  $c = (1, y_i, -x_i)$ . The table-leg locations are designed so that the position, tip and tilt frequencies are approximately the same: 1.72, 1.74, and 1.85 Hz. The vertical frequency responses at different locations on the table are plotted in Figure 11b, and what is apparent is that the shapes are the same but the magnitudes differ. The following 2nd response is a good approximation for any point on the table:

$$\frac{z}{f} = \frac{1}{m_{eff} s^2 + b_{eff} s + k_{eff}}$$

The “eff” subscripts indicate respectively the effective mass, damping, and spring constant. If an experimental object on the table top has resonant modes well above 1 Hz then the simple table model  $z/f = 1/(m_{eff}s^2)$  is a good approximation with just one parameter. As the table top location moves away from the center-of-mass the vertical response has both translation and rotation, hence more motion, and inversely, a smaller effective mass. Contour lines for the effective mass are plotted in Figure 11a. The effective mass is smallest at the upper left corner and is almost 8 times less than the total mass. The contour lines have slanted axes because the three-table combination is not symmetric.

The main effect of the optical table is to increase the piston mode of the combined PSA and table. This effect can be approximated as follows. The PSA piston motion is modeled as a moving mass of  $m = 209$  kg on an offload spring with a total spring constant of  $k = 3 \times 1.8e5 = 5.4e5$  N/m and a piston mode of  $f_o = \text{sqrt}(k/m)/(2\pi) = 8.09$  Hz. The effective mass of the table underneath the PSA is approximated as  $m_{eff} = 750$  kg, which changes the piston mode to  $f_o' = \text{sqrt}(k(1/m + 1/m_{eff}))/2\pi = 9.15$  Hz. Mystery solved.

## APPENDIX B: DATA TRACES AND MODEL PARAMETERS

Information is provided to recreate the plots in Figure 7 to Figure 9. The step and dwell frequency responses collected in the course of the study are called “traces” and numbered consecutively. The PSA FE model is the “429 model,” named for the delivery date of April 9, 2009. The feedback blocks in the Figure 6 block diagram are defined as follows:

$$H_b = (sb_b + k_b)I, \text{ dimension } 3 \times 3$$

$$H_o = \text{diag}(m_o s^2 + b_o s + k_o \quad b_d s + k_d \quad b_d s + k_d), \text{ dimension } 3 \times 3$$

$$H_c = (v_1 v_1^T + v_2 v_2^T)(m_c s^2 + k_c), 3 \times 3$$

$$v_1 = (0 \quad -1 \quad 1)^T / \sqrt{2} = \text{tip direction}, \quad v_2 = (2 \quad -1 \quad -1)^T / \sqrt{6} = \text{tilt direction}$$

$$k_s = (k_p + k_i / s + s k_r) f_s(s), \text{ where } f_s(s) \text{ is structural filter, dimension } 1 \times 1$$

Table 1: Model Parameters

Figure		$bb$ kg/sec	$kb$ N/m	$mo$ kg	$bo$ kg/sec	$ko$ N/m	$bd$ kg/sec	$kd$ N/m	$kp$ N/m	$ki$ N-sec/m	$kr$ N/m-sec
7	Actuator	0.5%	1e12	0	0.5%	.18e6	0.5%	0.18e6	0	0	0
8 left	Mirror	0.5%	1e12	25	4800	.14e6	0.5%	0.14e6	1.7e6	22e6	1000
8 right	Mirror	0.5%	1e12	0	1e4	7.5e6	250	0.25e6	0	2.36e8	0
9 left	Vibration	3000	3.5e6	0	1e4	7.5e6	50	0.18e6	0.9e6	30e6	1000
9 right	Vibration	3000	3.5e6	0	2000	5.5e6	0.5%	20e6	0	1.73e8	0

**Actuator response:** Figure 7 top and bottom. The data trace is 147. The dummy actuator voice coil calibration is 0.51 N per V. The accelerometer calibration is  $-1.00$  m/sec<sup>2</sup> per V. The table model and mirror correction are *not* used in the top plot. In the bottom plot the table model is combined with the PSA and the PSA mirror correction is used with  $mc = 5$  kg (+8%) and  $kc = 1e5$  N/m (+6%). Further parameters for all of the responses are in Table 1.

**Mirror response with voice coil actuator:** Figure 8 left side. The data is the average of traces 300–302. The shaker calibration is 0.102 N per V. The accelerometer calibration is  $-1.00$  m/sec<sup>2</sup> per V. The laser calibration is 8 microns per V. The table and the PSA mirror corrections are *not* used in the model for this and all other parts of Figure 8 and Figure 9. The structural filter is  $f_s(s) = (1.562s^2 + 51.05s + 1.668e5)/(s^2 + 40.84s + 1.668e5)$ .

**Mirror response with piezo actuator:** Figure 8 right side. The data is the average of traces 379–382 and 384. The shaker calibration is 0.051 N per V. The accelerometer calibration is  $-4.00$  m/sec<sup>2</sup> per V. The laser calibration is 8 microns per V. The structural filter is not used.

**Vibration transmission with voice coil actuator:** Figure 9 left side. The data is the average of traces 317–318 divided by the average of traces 426 and 429–431. The shaker calibration is 0.102 N per V. The accelerometer calibration is – 1.00 m/sec<sup>2</sup> per V. The laser calibration is 8 microns per V. The structural filter is  $f_s(s) = 628/(s + 628)$ .

**Vibration transmission with piezo actuator:** Figure 9 right side. The data is the average of traces 420-425 divided by the average of traces 310-311 and 314-315. The shaker calibration is 0.051 N per V. The accelerometer calibration is – 4.00 m/sec<sup>2</sup> per V. The laser calibration is 8 microns per V. The structural filter is not used.

## ACKNOWLEDGEMENTS

The work described in this paper was carried out in part at the Jet Propulsion Laboratory, California Institute of Technology, under contract with the National Aeronautics and Space Administration. The authors wish to thank the Thirty Meter Telescope Observatory Corporation for funding this work.

The TMT Project gratefully acknowledges the contribution of the following actuator manufactures: The Pilot Group for the Piezo Pump Actuator ([inquiries@the-pilot-group.com](mailto:inquiries@the-pilot-group.com)), Marjan Research ([mvjean@marjanresearch.com](mailto:mvjean@marjanresearch.com)), and the Jet Propulsion Laboratory ([www.jpl.nasa.gov](http://www.jpl.nasa.gov))

The TMT Project gratefully acknowledges the contributions of Vince Stephens and Richard Macek, both formerly of HYTEC, Inc, 110 Eastgate Drive, Los Alamos, NM, USA 87544. Vince Stephens developed the finite element of the primary segment assembly and Richard Macek modified the model based on static load tests conducted at HYTEC.

The TMT Project gratefully acknowledges the support of the TMT partner institutions. They are the Association of Canadian Universities for Research in Astronomy (ACURA), the California Institute of Technology and the University of California. This work was supported as well by the Gordon and Betty Moore Foundation, the Canada Foundation for Innovation, the Ontario Ministry of Research and Innovation, the National Research Council of Canada, the Natural Sciences and Engineering Research Council of Canada, the British Columbia Knowledge Development Fund, the Association of Universities for Research in Astronomy (AURA) and the U.S. National Science Foundation.

## REFERENCES

- [1] Nelson, J. and Sanders, G. H., “The Status of the Thirty Meter Telescope Project,” Proc. SPIE 7012, 70121A, (2008).
- [2] Ponslet, E., Blanco, D., Cho, M., Mast, T., Nelson, J., Ponchione, R. J., Sirota, M., Stephens, V., Stepp, L., Tubb, A., Williams, E. C., “Development of the Primary Mirror Segment Support Assemblies for the Thirty Meter Telescope,” Proc. SPIE 6273, E. Atad-Ettedgui; J. Antebi; D. Lemke, Editors, (2006)
- [3] Williams, E. C., Baffes C., Mast T., Nelson J., Platt B., Ponchione R. J., Ponslet E., Setoodeh S., Sirota M., Stephens V., Stepp L., Tubb A., “Advancement of the Segment Support System for the Thirty Meter Telescope Primary Mirror,” Proc. SPIE 7018 , E. Atad-Ettedgui; Dietrich Lemke, Editors, (2008)
- [4] Thompson, P. M., MacMynowski, D. G., and Sirota, M. J., “Control Analysis of the TMT Primary Segment Assembly,” Proc. SPIE 7012, (2008).
- [5] Thompson, P. M., MacMynowski, D. G., Colavita, M. M., Regehr, M. W., and Sirota, M. J., “Servo Design and Analysis for the Thirty Meter Telescope Primary Mirror Actuators,” Proc. SPIE 7733, (2010).
- [6] MacMynowski, D. G., Thompson, P. M., and Sirota, M. J., “Analysis of TMT Primary Mirror Control Structure Interaction,” Proc. SPIE 7017, (2008).
- [7] MacMynowski, D. G., Thompson, P. M., Shelton, C., and Roberts, Jr. L. C., “Robustness of Thirty Meter Telescope Primary Mirror Control,” Proc. SPIE 7733, (2010).